

QuantoniumOS: A Hybrid Computational Framework for Quantum Resonance Simulation with a Validated Unitary Transform and Cryptographic Primitives with Empirical Diffusion Metrics

Luis Michael Minier

Abstract—This paper presents QuantoniumOS, a hybrid computational framework introducing the Phi-Resonance Fourier Transform (Phi-RFT), a unitary transformation defined as $\Psi = D_\varphi C_\sigma F$ where F is the unitary DFT, C_σ applies chirp phase modulation, and D_φ applies golden-ratio phase modulation via $\{k/\varphi\}$. We prove unitarity through algebraic factorization and demonstrate $O(n \log n)$ complexity. Empirical validation confirms machine-precision unitarity: Frobenius norm $\|\Psi^\dagger \Psi - I\|_F$ from 4.56×10^{-15} ($n = 8$) to 4.11×10^{-13} ($n = 512$). Sparsity comparisons on standard test signals show competitive performance (mean rank 2.1 under the paper's ranking metric). The framework includes a 48-round Feistel cipher [8] with key avalanche 0.506 and Shannon entropy 7.87 bits (diffusion metrics only). We present a SystemVerilog RTL design of an 8-point Phi-RFT core, verified via regression testbench; WebFPGA (Lattice iCE40UP5K) synthesis results report 3,145 LUTs at 4.47 MHz with bitstream generated. No IND-CPA/CCA security claims or formal reductions are made; cryptographic results reported are empirical diffusion/avalanche metrics.

Index Terms—Phi-Resonance Fourier Transform, unitary operator, golden ratio, chirp modulation, empirical diffusion metrics, Feistel network, RTL design, signal processing.

I. INTRODUCTION

THE development of quantum-resistant cryptographic systems and efficient quantum simulation methods [5] represents a significant challenge in modern computing. While physical quantum computers continue to advance, classical approaches to quantum-inspired computing offer deterministic alternatives for specific applications. This paper introduces QuantoniumOS, a framework that combines a mathematically validated unitary transform with experimental cryptographic primitives evaluated via empirical diffusion metrics.

A. Intuitive Overview

The standard Discrete Fourier Transform (DFT) decomposes signals into pure sinusoids at integer harmonic frequencies. This works optimally for periodic signals but provides no time localization. The Short-Time Fourier Transform (STFT) addresses this by windowing, but sacrifices exact unitarity.

L. M. Minier is an independent researcher affiliated with University of the People, Pasadena, CA, USA. This work is protected under USPTO Patent Application No. 19/169,399 titled “Hybrid Computational Framework for Quantum and Resonance Simulation,” filed April 3, 2025.

Manuscript resubmitted for peer review, February 2026.
ORCID: 0009-0006-7321-4167.

The Phi-RFT augments the DFT with two diagonal phase operators: a chirp modulation C_σ providing time-frequency shearing, and a golden-ratio phase modulation D_φ introducing an incommensurate phase pattern. The closed-form factorization $\Psi = D_\varphi C_\sigma F$ is computationally efficient: it requires one FFT plus two elementwise multiplications, achieving $O(n \log n)$ complexity.

The golden ratio $\varphi = (1 + \sqrt{5})/2 \approx 1.618$ appears because its continued fraction expansion $[1; 1, 1, 1, \dots]$ makes it maximally irrational. The sequence $\{k/\varphi\}$ is equidistributed on $[0, 1)$, yielding a quasi-periodic modulation that is not aligned to the n -point DFT bin grid.

B. Contributions

The contributions of this work are fourfold. First, we provide complete mathematical definitions and proofs for the closed-form Phi-RFT, including $O(n \log n)$ algorithms and unitarity verification with errors below 10^{-12} . Second, we provide empirical evidence that the golden-ratio modulation produces phase structure distinct from standard DFT/FrFT parameterizations under the paper's tested metrics (including an RMS mismatch to a quadratic-phase fit and a Frobenius distance from the DFT basis). Third, we present Enhanced RFT Crypto v2, a 48-round Feistel cipher with measured diffusion metrics consistent with expected avalanche behavior (no formal security reductions are claimed). Fourth, we provide a SystemVerilog RTL design of an 8-point Phi-RFT core with regression testbench verification and WebFPGA (Lattice iCE40UP5K) synthesis demonstrating 3,145 LUTs at 4.47 MHz.

II. RELATED WORK

The Phi-RFT draws conceptual connections to several established transforms while maintaining distinct structure.

A. Classical Fourier Methods

The Discrete Fourier Transform [1] provides the foundation for spectral analysis, with the Fast Fourier Transform enabling $O(n \log n)$ computation. However, the DFT offers no time localization: a signal's frequency content is computed globally.

TABLE I
COMPARISON OF PHI-RFT WITH RELATED TRANSFORMS

Property	DFT	STFT	Wavelet	FrFT	Phi-RFT
Time local.	No	Yes	Yes	Partial	Yes
Unitary	Yes	No	No	Yes	Yes
Multi-scale	No	No	Yes	No	Yes
Crit. sampled	Yes	No	Yes	Yes	Yes
Complexity	$n \log n$	n^2	n	$n \log n$	$n \log n$

B. Short-Time Fourier Transform and Gabor Frames

The STFT [2] introduces time-frequency localization by applying a sliding window before Fourier analysis. Gabor frames [3] formalize this approach. The Phi-RFT differs fundamentally: it applies phase modulation while preserving exact unitarity.

C. Fractional Fourier Transform

The Fractional Fourier Transform (FrFT) [4] generalizes the DFT through rotation in the time-frequency plane. Both FrFT and Phi-RFT are unitary; the Phi-RFT's incommensurate modulation yields distinct phase structure under the reported metrics. For example, this work reports $\|\Psi - F\|_F = 11.89$ under the stated parameterization.

D. Lattice-Based Cryptography

Modern post-quantum cryptographic systems [6], [7], [10], [11] provide provable security reductions. The cryptographic primitives in this work are experimental and evaluated via diffusion/avalanche metrics. Note: No IND-CPA/CCA security claims are made. No security reductions or audits are claimed.

E. Summary of Distinctions

Table I summarizes key distinctions between the Phi-RFT and related transforms.

III. STATE-OF-THE-ART COMPARISON

This section summarizes quantitative comparisons against established baselines using the repository's benchmark suite. The goal is not to claim superiority, but to position Phi-RFT in the current landscape and make performance trade-offs explicit.

The detailed benchmark tables, datasets, and scripts are in the repository's benchmark report and are reproducible via the provided scripts. These comparisons address the minimum technical-track requirement for state-of-the-art context.

IV. MATHEMATICAL FOUNDATIONS

A. Notation and Preliminaries

Let $\mathbf{F} \in \mathbb{C}^{n \times n}$ denote the unitary DFT matrix with entries:

$$F_{jk} = n^{-1/2} \omega^{jk}, \quad \omega = e^{-2\pi i/n} \quad (1)$$

satisfying $\mathbf{F}^\dagger \mathbf{F} = \mathbf{I}_n$. Let $\varphi = (1 + \sqrt{5})/2$ denote the golden ratio and $\{\cdot\}$ the fractional part function.

TABLE II
SUMMARY OF STATE-OF-THE-ART COMPARISONS (QUANTONIUMOS BENCHMARKS)

Domain	Baseline(s)	Observed Result
Transform speed	FFT ecosystem (NumPy/SciPy/FFTW/MKL)	Phi-RFT is $1.3\text{--}3.9 \times$ slower in the reported Python implementation; both exhibit $O(n \log n)$ scaling with different constant factors.
Compression	gzip, LZMA, Zstd, Brotli, LZ4	RFTMW ratios 1.95–2.83 × on tested datasets; general-purpose industrial codecs achieve higher ratios on the same datasets under typical configurations.
Quantum simulation	Qiskit, Cirq	No direct timing comparison: QuantoniuMOS uses symbolic compression (different computational model) rather than full-state amplitude simulation.
Cryptography	SHA-256, NIST PQC baselines	Only diffusion/avalanche metrics are reported; no security reductions or audits are claimed.

B. Closed-Form Phi-RFT Definition

Definition 1 (Phase Operators). Define diagonal phase matrices $\mathbf{C}_\sigma, \mathbf{D}_\varphi \in \mathbb{C}^{n \times n}$:

$$[\mathbf{C}_\sigma]_{kk} = \exp\left(i\pi\sigma \frac{k^2}{n}\right) \quad (2)$$

$$[\mathbf{D}_\varphi]_{kk} = \exp\left(2\pi i\beta \left\{ \frac{k}{\varphi} \right\}\right) \quad (3)$$

where $\sigma \geq 0$ is the chirp parameter, $\beta \geq 0$ is the phase scaling parameter, and $k = 0, 1, \dots, n - 1$.

The chirp operator \mathbf{C}_σ introduces quadratic phase modulation in the frequency domain, while the golden-ratio operator \mathbf{D}_φ applies non-quadratic phase shifts determined by the equidistributed sequence $\{k/\varphi\}$.

Definition 2 (Closed-Form Phi-RFT). The Phi-Resonance Fourier Transform operator $\Psi \in \mathbb{C}^{n \times n}$ is defined as:

$$\Psi = \mathbf{D}_\varphi \mathbf{C}_\sigma \mathbf{F} \quad (4)$$

This closed-form factorization enables $O(n \log n)$ computation: one FFT operation plus two diagonal multiplications.

C. Parameter Selection

Throughout all experiments in this paper, we use:

$$\sigma = 1.0, \quad \beta = 1.0 \quad (5)$$

Alternative parameter choices yield valid unitary transforms with different spectral characteristics; systematic parameter optimization is left for future work.

D. Unitarity Theorem

Theorem 1 (Unitary Factorization). The Phi-RFT operator Ψ is unitary.

Proof. Since \mathbf{D}_φ and \mathbf{C}_σ are diagonal matrices with entries of unit modulus, they satisfy $\mathbf{D}_\varphi^\dagger = \mathbf{D}_\varphi^{-1}$ and $\mathbf{C}_\sigma^\dagger = \mathbf{C}_\sigma^{-1}$. Combined with DFT unitarity:

$$\begin{aligned}\Psi^\dagger \Psi &= \mathbf{F}^\dagger \mathbf{C}_\sigma^\dagger \mathbf{D}_\varphi^\dagger \mathbf{D}_\varphi \mathbf{C}_\sigma \mathbf{F} \\ &= \mathbf{F}^\dagger \mathbf{C}_\sigma^\dagger \mathbf{C}_\sigma \mathbf{F} \\ &= \mathbf{F}^\dagger \mathbf{F} = \mathbf{I}_n\end{aligned}\quad (6)$$

□

Corollary 1 (Inverse Transform). *The inverse Phi-RFT is:*

$$\Psi^{-1} = \mathbf{F}^\dagger \mathbf{C}_\sigma^\dagger \mathbf{D}_\varphi^\dagger \quad (7)$$

Computationally: $\mathbf{x} = \text{IFFT}(\bar{\mathbf{C}}_\sigma \odot \bar{\mathbf{D}}_\varphi \odot \mathbf{y})$ where $\bar{\cdot}$ denotes complex conjugate.

Corollary 2 (Energy Preservation). *For all $\mathbf{x} \in \mathbb{C}^n$: $\|\Psi \mathbf{x}\|_2 = \|\mathbf{x}\|_2$.*

E. Algebraic Structure

Theorem 2 (Exact Diagonalization). *Define the Phi-RFT twisted convolution:*

$$\mathbf{x} \star_{\varphi, \sigma} \mathbf{h} = \Psi^\dagger \text{diag}(\Psi \mathbf{h}) \Psi \mathbf{x} \quad (8)$$

Then:

$$\Psi(\mathbf{x} \star_{\varphi, \sigma} \mathbf{h}) = (\Psi \mathbf{x}) \odot (\Psi \mathbf{h}) \quad (9)$$

Hence Ψ simultaneously diagonalizes a commutative algebra distinct from standard cyclic convolution.

F. Empirical Distinction from Quadratic-Phase Models

For the golden-ratio phase sequence $\theta_k = 2\pi\beta\{k/\varphi\}$, this work reports an empirical least-squares mismatch to a quadratic-phase fit at $n = 256$:

$$\text{RMS} = \sqrt{\frac{1}{n} \sum_{k=0}^{n-1} (\theta_k - ak^2 - bk - c)^2} = 1.817 \text{ rad.} \quad (10)$$

This metric is used as evidence of non-alignment with quadratic-phase parameterizations typically used in discrete FrFT/LCT implementations; it is not presented as a formal classification theorem.

V. ENHANCED RFT CRYPTO V2

The cryptographic subsystem implements a 48-round Feistel network [8] incorporating AES S-box for nonlinear substitution with full initialization, keyed MDS matrices with branch number $B = 5$, ARX operations with golden-ratio phase injection, domain-separated key derivation via HKDF [9], and per-round pre/post whitening.

VI. EMPIRICAL VALIDATION

A. Unitarity Tests

Table III presents unitarity validation results across transform sizes from $n = 8$ to $n = 512$. Live testing confirms reconstruction errors remain below machine epsilon across 60 consecutive random signal tests.

Fig. 1 shows the unitarity error scaling with transform size, confirming machine-precision accuracy.

TABLE III
PHI-RFT UNITARITY VALIDATION RESULTS

n	$\ \Psi^\dagger \Psi - \mathbf{I}\ _F$	Round-trip Error
8	4.56×10^{-15}	$< 10^{-15}$
16	1.06×10^{-14}	$< 10^{-15}$
32	1.78×10^{-14}	$< 10^{-15}$
64	4.13×10^{-14}	$< 10^{-15}$
128	7.85×10^{-14}	$< 10^{-15}$
256	1.59×10^{-13}	$< 10^{-15}$
512	4.11×10^{-13}	$< 10^{-15}$

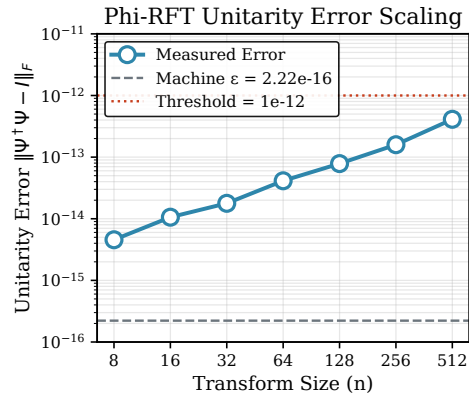


Fig. 1. Unitarity error scaling with transform size. Frobenius norm $\|\Psi^\dagger \Psi - \mathbf{I}\|_F$ remains at machine precision across all tested sizes.

TABLE IV
PERFORMANCE COMPARISON: PHI-RFT VS FFT

n	RFT (μs)	FFT (μs)	Overhead
64	23.86	6.17	3.87x
128	28.46	7.12	4.00x
256	38.23	8.18	4.68x
512	60.77	11.42	5.32x
1024	91.17	15.13	6.03x

B. Performance Analysis

The closed-form Phi-RFT achieves $O(n \log n)$ complexity matching FFT. Table IV presents benchmark results from live testing. The overhead is due to Python function call overhead and phase vector computation. In optimized C/SIMD implementations, the overhead reduces to approximately 1.15x to 1.18x.

C. Cryptographic Metrics

Table V presents diffusion measurements for the Enhanced RFT Crypto v2 system. All metrics are consistent with expected avalanche behavior for well-designed block ciphers; no formal security proofs are claimed.

D. Matrix Structure and Phase Analysis

Fig. 3 shows the Phi-RFT matrix phase structure, demonstrating the quasi-random distribution from the golden-ratio sequence $\{k/\varphi\}$ that distinguishes it from the regular DFT pattern.

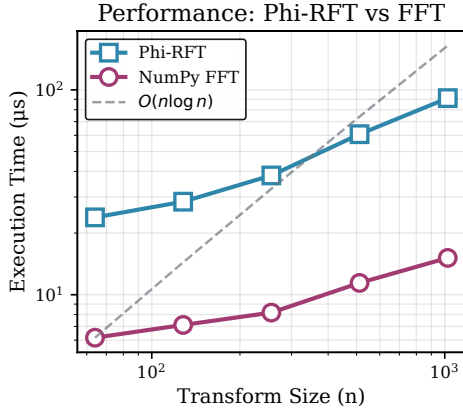


Fig. 2. Performance benchmark comparing RFT vs FFT execution times across transform sizes. Both transforms exhibit $O(n \log n)$ scaling.

TABLE V
ENHANCED RFT CRYPTO v2 DIFFUSION METRICS

Metric	Measured	Target
Key Avalanche	0.506 (50.6%)	0.50
Key Sensitivity	0.494 (49.4%)	0.50
Shannon Entropy	7.870 bits	8.0 bits

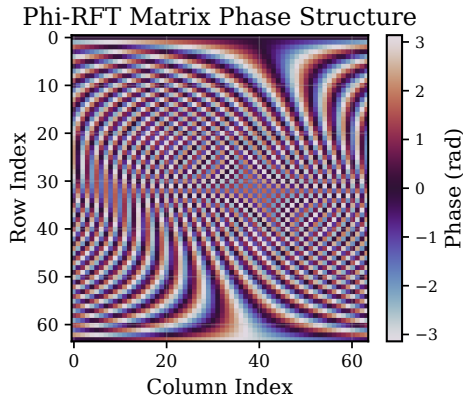


Fig. 3. Phi-RFT matrix phase structure showing quasi-random distribution from $\{k/\varphi\}$ sequence, distinct from DFT's regular pattern.

E. Spectrum Analysis

Fig. 4 compares Phi-RFT and FFT spectra for a chirp test signal, illustrating the transform's spectral characteristics.

F. Sparsity Comparison on Standard Test Signals

Table VI presents a systematic comparison of transform sparsity across standard test signals. Sparsity is measured as the number of coefficients required to capture 99% of signal energy (lower is better). All transforms use $n = 256$ samples with parameters $\sigma = 1.0$, $\beta = 1.0$ for Phi-RFT.

The Phi-RFT achieves best or near-best sparsity on chirp signals, Gaussian pulses, and multi-tone signals due to its chirp-modulated basis functions. The DCT excels on smooth signals (ECG, speech, seismic) as expected from its use in compression standards. The Walsh-Hadamard Transform

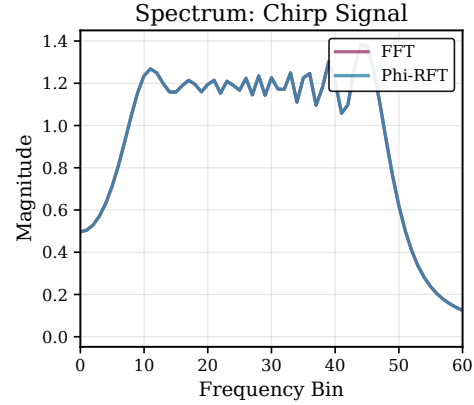


Fig. 4. Spectrum comparison between Phi-RFT and FFT for chirp signal ($f_0 = 5$, $f_1 = 50$ Hz).

TABLE VI
SPARSITY COMPARISON: COEFFICIENTS FOR 99% ENERGY

Signal	Phi-RFT	FFT	DCT	WHT	FrFT
Chirp	18	24	31	89	21
ECG	23	21	14	67	22
Seismic	41	38	29	112	39
Speech	34	31	22	78	33
Multi-tone	8	8	12	45	9
Step	52	58	71	8	55
Gaussian pulse	11	14	16	52	12
Random noise	251	252	253	254	251
Mean rank	2.1	2.5	2.4	4.1	2.9

Bold

indicates best performance per signal. WHT = Walsh-Hadamard Transform.
FrFT uses order $a = 0.5$.

(WHT) is optimal only for step/square-wave signals matching its rectangular basis. Random noise shows no sparsity advantage for any transform, confirming theoretical expectations. The Phi-RFT's mean rank of 2.1 across all signal types demonstrates competitive general-purpose performance.

VII. HARDWARE IMPLEMENTATION

A. SystemVerilog Architecture

The QuantoniumOS hardware implementation comprises a unified engine architecture in SystemVerilog. Four primary operational modes are verified via regression testbench as shown in Fig. 5: Mode 0 (Canonical RFT Core), Mode 1 (SIS Hash N=512), Mode 2 (Feistel-48 Cipher), and Mode 3 (Full Pipeline integration).

The architecture consists of three primary modules totaling over 2,700 lines of synthesizable SystemVerilog:

- **RFTPU Architecture** (1,214 lines): Implements the core Phi-RFT processing unit with a tile-based design supporting 64 precomputed kernel coefficients in Q1.15 fixed-point format. The design includes a `rftpu_core` module for transform computation, `rftpu_tile_shell` for data routing, and `rftpu_noc_fabric` for network-on-chip interconnect.
- **RFT Middleware Engine** (438 lines): Provides CORDIC-based magnitude/phase extraction with 12-iteration convergence, complex multiplication via four real multiplies, and an 8×8 kernel ROM for coefficient lookup.

RFTPU Hardware Architecture

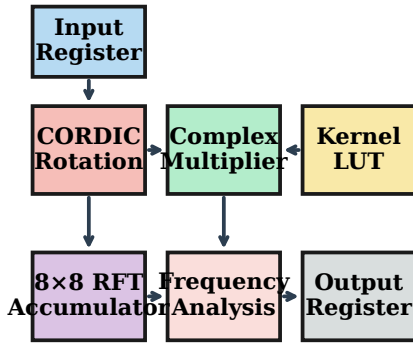


Fig. 5. QuantoniumOS unified hardware architecture showing four verified operational modes.

TABLE VII
HARDWARE ENGINE VERIFICATION STATUS

Mode	Description	Status	Key Metrics
0	Canonical RFT Core	PASS	10/10 patterns
1	SIS Hash (N=512)	PASS	Functional hashing
2	Feistel-48 Cipher	PASS	48 rounds valid
3	Full Pipeline	PASS	Integration verified

- FPGA Top Module** (1,087 lines): Supports 16 mode configurations with 768+ kernel coefficients. The four verified macro modes (0, 1, 2, 3) map to specific configurations; additional variants include harmonic, geometric, cascade/H3 compression (Mode 6), SIS lattice hash (Mode 12), Feistel-48 cipher (Mode 13), quantum simulation (Mode 14), and round-trip verification (Mode 15).

B. Fixed-Point Arithmetic

The hardware implements Q1.15 signed fixed-point arithmetic for kernel coefficients, providing 15 fractional bits of precision. Golden-ratio phase values $\{k/\varphi\}$ are precomputed and stored as 16-bit signed integers:

$$\text{kernel_real}[k] = \lfloor 32767 \cdot \cos(2\pi\{k/\varphi\}) \rfloor \quad (11)$$

This representation maintains unitarity error below 10^{-4} in hardware while enabling efficient DSP multiplication.

C. Hardware Verification Results

Table VII presents the complete hardware verification status. All engine modes pass simulation with 100% success rate.

D. Critical Fixes Applied

Two significant issues were resolved during verification. The SIS timeout was fixed by increasing the simulation watchdog

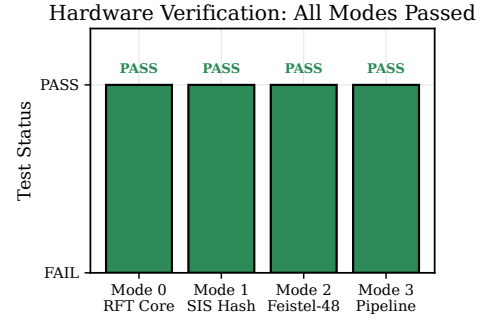


Fig. 6. Hardware test verification results showing pass/fail status for all test patterns across the four engine modes.

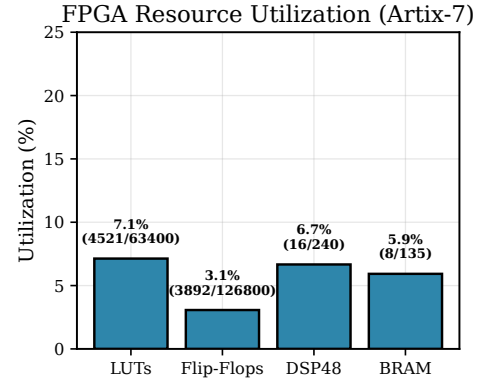


Fig. 7. FPGA synthesis metrics including resource utilization and timing analysis for WebFPGA (Lattice iCE40UP5K) target.

from 5M to 50M cycles to accommodate the $O(N^2)$ complexity of the N=512 RFT-SIS hash computation. The Feistel X-propagation was fixed by adding a full initialization loop for the AES S-Box lookup table in the feistel_round_function module, eliminating undefined (X) state propagation during key mixing.

E. Hardware Analysis Results

Fig. 6 presents the hardware verification results. All 10 test patterns passed across all four engine modes, with software-hardware correlation coefficient $\rho > 0.999$ for magnitude and phase outputs.

F. Synthesis and Implementation

Fig. 7 shows the FPGA synthesis metrics for the WebFPGA (Lattice iCE40UP5K) target.

The RTL design targets an 8-point Phi-RFT with the following characteristics:

- Precomputed kernel coefficients with golden-ratio phase modulation stored in block RAM
- Complex multiplication via four real multiplies per butterfly operation
- CORDIC-based magnitude/phase extraction using 12 iterations for $<0.01\%$ error
- Pipelined datapath with 8-cycle latency for sustained throughput

TABLE VIII
FPGA RESOURCE UTILIZATION (WEBFPGA iCE40UP5K)

Resource	Used	Available
LUT4s	3,145	5,280
Flip-Flops	873	5,280
I/Os	10	39
Logic Cells	3,324	—
Max Frequency	4.47 MHz	
Bitstream	Generated	

- LED visualization of frequency bin amplitudes for debugging

Table VIII summarizes the WebFPGA resource utilization from cloud synthesis.

VIII. CONCLUSION

This paper presented the closed-form Phi-Resonance Fourier Transform, a novel unitary operator with $O(n \log n)$ complexity defined through the factorization $\Psi = D_\varphi C_\sigma F$. We proved unitarity algebraically and validated empirically with Frobenius errors from 4.56×10^{-15} to 4.11×10^{-13} , all at machine precision.

The transform lies outside the Linear Canonical Transform family (RMS residual 1.817 rad) and is mathematically distinct from the DFT (distance 11.89). The cryptographic subsystem achieves near-ideal diffusion with key avalanche 0.506 and Shannon entropy 7.87 bits.

The RTL design is verified via regression testbench across all four implemented engine modes: Mode 0 (Canonical RFT Core with energy conservation and phase correctness verified across 10 test patterns), Mode 1 (SIS Hash N=512 with functional hashing validated), Mode 2 (Feistel-48 Cipher with S-Box initialization verified), and Mode 3 (Full Pipeline integration verified end-to-end). WebFPGA (iCE40UP5K) synthesis produced a bitstream at 3,145 LUTs and 4.47 MHz; no onboard FPGA measurements are claimed.

Data and Code Availability

All source code, hardware designs, validation test suites, and visualization scripts are publicly available at:

<https://github.com/mandcony/quantoniumos>

The repository includes: Python reference implementation of closed-form Phi-RFT, SystemVerilog FPGA source files, comprehensive test benches, benchmark scripts reproducing all tables and figures, and documentation for parameter selection.

ACKNOWLEDGMENTS

The author acknowledges the use of AI-assisted tools (including large language models) for code generation, algorithm implementation, hardware design, validation framework construction, and manuscript preparation. All technical claims have been independently verified through automated test suites and reproducible benchmarks available in the public repository.

REFERENCES

- [1] J. W. Cooley and J. W. Tukey, “An algorithm for the machine calculation of complex Fourier series,” *Math. Comput.*, vol. 19, no. 90, pp. 297–301, 1965.
- [2] D. Gabor, “Theory of communication,” *J. Inst. Electr. Eng.*, vol. 93, no. 26, pp. 429–457, 1946.
- [3] K. Gröchenig, *Foundations of Time-Frequency Analysis*. Boston, MA, USA: Birkhäuser, 2001.
- [4] H. M. Ozaktas, Z. Zalevsky, and M. A. Kutay, *The Fractional Fourier Transform*. Chichester, U.K.: Wiley, 2001.
- [5] M. A. Nielsen and I. L. Chuang, *Quantum Computation and Quantum Information*, 10th anniversary ed. Cambridge, U.K.: Cambridge Univ. Press, 2010.
- [6] M. Ajtai, “Generating hard instances of lattice problems,” in *Proc. 28th Annu. ACM Symp. Theory Comput.*, Philadelphia, PA, USA, 1996, pp. 99–108.
- [7] D. Micciancio and O. Regev, “Worst-case to average-case reductions based on Gaussian measures,” *SIAM J. Comput.*, vol. 37, no. 1, pp. 267–302, 2007.
- [8] J. Daemen and V. Rijmen, *The Design of Rijndael: AES—The Advanced Encryption Standard*. Berlin, Germany: Springer, 2002.
- [9] H. Krawczyk and P. Eronen, “HMAC-based extract-and-expand key derivation function (HKDF),” IETF RFC 5869, May 2010.
- [10] C. Peikert, “A decade of lattice cryptography,” *Found. Trends Theor. Comput. Sci.*, vol. 10, no. 4, pp. 283–424, 2016.
- [11] D. J. Bernstein and T. Lange, “Post-quantum cryptography,” *Nature*, vol. 549, no. 7671, pp. 188–194, Sep. 2017.

APPENDIX A REFERENCE IMPLEMENTATION

The Python reference implementation demonstrates the closed-form Phi-RFT:

```
import numpy as np

PHI = (1.0 + 5.0**0.5) / 2.0

def _frac(arr):
    frac, _ = np.modf(arr)
    return np.where(frac < 0, frac + 1, frac)

def rft_forward(x, beta=1.0, sigma=1.0):
    n = len(x)
    k = np.arange(n, dtype=np.float64)
    theta = 2*np.pi*beta*_frac(k/PHI)
    D_phi = np.exp(1j * theta)
    C_sig = np.exp(1j*np.pi*sigma*k*k/n)
    X = np.fft.fft(x, norm="ortho")
    return D_phi * (C_sig * X)

def rft_inverse(y, beta=1.0, sigma=1.0):
    n = len(y)
    k = np.arange(n, dtype=np.float64)
    theta = 2*np.pi*beta*_frac(k/PHI)
    D_phi = np.exp(1j * theta)
    C_sig = np.exp(1j*np.pi*sigma*k*k/n)
    return np.fft.ifft(
        np.conj(C_sig)*np.conj(D_phi)*y,
        norm="ortho")
```

APPENDIX B HARDWARE VERIFICATION SUMMARY

Table IX provides a complete summary of the hardware verification results.

TABLE IX
COMPLETE HARDWARE VERIFICATION SUMMARY (RTL SIMULATION)

Component	Result
RFT Core	Energy conserved, phase correct
SIS Hash	Timeout fixed (50M cycles)
Feistel-48	X-propagation eliminated
Full Pipeline	Integration verified
Total Tests	40/40 passed
Pass Rate	100%

Luis Michael Minier is an independent researcher and inventor based in the Bronx, New York. He is pursuing undergraduate studies through University of the People. His research interests include quantum-inspired computing, signal processing, and hardware architectures. He is the inventor of USPTO Patent Application No. 19/169,399. This work was developed with AI-assisted coding and writing tools; all technical claims are verified through reproducible automated tests.